Redox Biology 20 (2019) 458–466

Contents lists available at ScienceDirect

Redox Biology

journal homepage: www.elsevier.com/locate/redox

Research Paper

Enhanced inter-compartmental Ca^{2+} flux modulates mitochondrial metabolism and apoptotic threshold during aging

Corina T. Madreiter-Sokolowski[a,b,*], Markus Waldeck-Weiermair[a], Marie-Pierre Bourguignon[c], Nicole Villeneuve[c], Benjamin Gottschalk[a], Christiane Klec[d], Sarah Stryeck[a], Snjezana Radulovic[a], Warisara Parichatikanond[e], Saša Frank[a], Tobias Madl[a], Roland Malli[a,f], Wolfgang F. Graier[a,f,**]

[a] Molecular Biology and Biochemistry, Gottfried Schatz Research Center, Medical University of Graz, Neue Stiftingtalstraße 6/6, 8010 Graz, Austria
[b] Department of Health Sciences and Technology, ETH Zurich, Schorenstrasse 16, 8603 Schwerzenbach, Switzerland
[c] Servier Research Institute, Cardiovascular Unit, 11 rue des Moulineaux, 92150 Suresnes, France
[d] Division of Oncology, Medical University of Graz, Auenbruggerplatz 15, 8036 Graz, Austria
[e] Department of Pharmacology, Faculty of Pharmacy, Mahidol University, Bangkok, Thailand
[f] BioTechMed, Graz, Austria

ARTICLE INFO

Keywords:
Mitochondria
Endoplasmic reticulum
Calcium signaling
ER-mitochondrial coupling
Vascular aging

ABSTRACT

Background: Senescence is characterized by a gradual decline in cellular functions, including changes in energy homeostasis and decreased proliferation activity. As cellular power plants, contributors to signal transduction, sources of reactive oxygen species (ROS) and executors of programmed cell death, mitochondria are in a unique position to affect aging-associated processes of cellular decline. Notably, metabolic activation of mitochondria is tightly linked to Ca^{2+} due to the Ca^{2+} -dependency of several enzymes in the Krebs cycle, however, overload of mitochondria with Ca^{2+} triggers cell death pathways. Consequently, a machinery of proteins tightly controls mitochondrial Ca^{2+} homeostasis as well as the exchange of Ca^{2+} between the different cellular compartments, including Ca^{2+} flux between mitochondria and the endoplasmic reticulum (ER).

Methods: In this study, we investigated age-related changes in mitochondrial Ca^{2+} homeostasis, mitochondrial-ER linkage and the activity of the main ROS production site, the mitochondrial respiration chain, in an *in vitro* aging model based on porcine aortic endothelial cells (PAECs), using high-resolution live cell imaging, proteomics and various molecular biological methods.

Results: We describe that in aged endothelial cells, increased ER-mitochondrial Ca^{2+} crosstalk occurs due to enhanced ER-mitochondrial tethering. The close functional inter-organelle linkage increases mitochondrial Ca^{2+} uptake and thereby the activity of the mitochondrial respiration, but also makes senescent cells more vulnerable to mitochondrial Ca^{2+}-overload-induced cell death. Moreover, we identified the senolytic properties of the polyphenol resveratrol, triggering cell death via mitochondrial Ca^{2+} overload exclusively in senescent cells.

Conclusion: By unveiling aging-related changes in the inter-organelle tethering and Ca^{2+} communications we have advanced the understanding of endothelial aging and highlighted a potential basis to develop drugs specifically targeting senescent cells.

1. Introduction

The hallmark of aging is a progressive decline in the ability of an organism to counteract stress, damage and disease, resulting in impaired physiological function, pathologies and, ultimately, death [1]. On the cellular level the process of aging is accompanied by a decreased proliferation rate, increased endoplasmic reticulum (ER) stress and production of potentially harmful reactive oxygen species (ROS) [2]. As central hubs for energy production, Ca^{2+} homeostasis, cell signaling as well as for apoptosis, mitochondria are crucially involved in these aging processes [3]. *In vitro* and *in vivo* experiments revealed dramatic alterations in mitochondrial function during aging [4]. Changes in mitochondrial activity during senescence have been associated with increased mitochondrial ROS production, causing cellular damage of

* Corresponding author at: Department of Health Sciences and Technology, ETH Zurich, Schorenstrasse 16, 8603 Schwerzenbach, Switzerland.
** Corresponding author at: Gottfried Schatz Research Center, Molecular Biology and Biochemistry, Medical University of Graz, Neue Stiftingtalstraße 6/6, 8010 Graz, Austria.
E-mail addresses: corina.madreiter@hest.ethz.ch (C.T. Madreiter-Sokolowski), wolfgang.graier@medunigraz.at (W.F. Graier).

https://doi.org/10.1016/j.redox.2018.11.003
Received 11 October 2018; Received in revised form 2 November 2018; Accepted 6 November 2018
Available online 09 November 2018

mitochondrial and nuclear DNA and advancing aging-related diseases [5]. Consistent with this, lifespan-prolonging interventions, such as caloric restriction, are frequently linked to a decrease in overall energy production [6]. Furthermore, reduction of mitochondrial content *in vivo* has been reported to reduce the spectrum of senescence effectors and phenotypes in mice [7], highlighting the overall harmful role of mitochondria in cellular senescence.

In order to reveal mitochondrial targets for therapeutic interventions against age-related diseases, we need to understand aging-associated mitochondrial changes to elaborate potential interventions that allow fine-tuning of mitochondrial activity. One potential regulator of mitochondrial activity in aging is the second messenger Ca^{2+}. By stimulating Ca^{2+}-dependent dehydrogenases of the tricarboxylic acid (TCA) cycle, Ca^{2+} boosts the activity of the mitochondrial respiration chain and, thereby, mitochondrial adenosine triphosphate (ATP) production via oxidative phosphorylation [8]. By stimulating the mitochondrial respiration chain, matrix Ca^{2+} also keeps mitochondrial membrane potential, which gets temporarily dissipated by entering Ca^{2+}, stable. However, in case of overwhelming mitochondrial Ca^{2+} accumulation, permeability of the inner mitochondrial membrane increases drastically, resulting in the dissipation of mitochondrial membrane potential, shutdown of mitochondrial respiration and finally initiation of cell death signaling pathways [9,10].

Due to its critical role in the cells' most crucial physiological processes, energy supply and cell death, mitochondrial Ca^{2+} uptake is tightly controlled by various proteins [11]. Mitochondria also buffer cytosolic Ca^{2+} elevations caused by influx through plasma membrane Ca^{2+} channels [12] or by depletion of the biggest internal Ca^{2+} store, the ER [13]. In regions of so-called mitochondria-associated ER membranes (MAMs), mitochondria are in close proximity to the ER and sophisticated toolkits are localized there to ensure Ca^{2+} trafficking between these organelles [14]: The sarco/ER Ca^{2+} ATPases (SERCAs) actively pump Ca^{2+} from the cytosol into the lumen of the ER upon cleavage of ATP, thus serving as a functional damper to inositol-1,4,5 trisphosphate (IP_3)-induced intracellular Ca^{2+} release from the IP_3 receptors (IP_3Rs) [15]. Once cytosolic Ca^{2+} levels rise due to ER Ca^{2+} depletion or external Ca^{2+} entry, mitochondria take up Ca^{2+} rapidly via the voltage-dependent anion channel (VDAC) in the outer mitochondrial membrane (OMM). Tightly controlled machineries of heterogenic and cell-type-specific protein complexes control mitochondrial Ca^{2+} uptake via the mitochondrial Ca^{2+} uniporter (MCU) complex in the inner mitochondrial membrane (IMM) [16]. The structural linkage between ER and mitochondria is also strongly regulated by various proteins that establish a proper connection between ER and mitochondria, including the protein kinase A (PKA)-anchoring proteins Rab32 and A-kinase anchor proteins (AKAP) as well as mitofusin 2 (MFN2) and glucose-regulated protein 75 (GRP75) [17].

Notably, changes in mitochondrial Ca^{2+} homeostasis as well as in the ER-mitochondria crosstalk have been reported to modulate a cell's ability to adapt to stress and to counteract cellular damage [18], both processes known to be disturbed during senescence [2]. Accordingly, the current study was designed to investigate age-related changes in mitochondrial Ca^{2+} homeostasis and their impact on mitochondrial and cellular function in an *in vitro* aging model based upon successive passages of porcine aortic endothelial cells (PAECs).

2. Methods

2.1. Chemicals and buffer solutions

Cell culture materials were obtained from PAA laboratories (Pasching, Austria) or Sigma Aldrich (Vienna, Austria). Prior to live-cell experiments, cells were washed and maintained for 20 min in a HEPES-buffered solution containing 138 mM NaCl, 5 mM KCl, 2 mM $CaCl_2$, 1 mM $MgCl_2$, 1 mM HEPES, 2.6 mM $NaHCO_3$, 0.44 mM KH_2PO_4, 0.34 mM Na_2HPO_4, 1 mM D-glucose, 0.1% vitamins, 0.2% essential amino acids and 1% penicillin-streptomycin, the pH of which was adjusted to 7.4 with NaOH or HCl. During the live cell imaging experiments cells were perfused with a Ca^{2+}-containing buffer, which consisted of 145 mM NaCl, 5 mM KCl, 2 mM $CaCl_2$, 1 mM $MgCl_2$, 10 mM D-glucose and 10 mM HEPES, pH adjusted to 7.4.

2.2. Cell culture and transfection

PAECs were isolated from the thoracic part of porcine aorta as described in by scraping [19] and cultured in collagen I-coated 175 cm^2 flasks (Becton Dickinson; New Jersey, U.S.) in Dulbecco's Modified Eagle's Medium (DMEM) (Sigma-Aldrich; Vienna, Austria) containing 10% fetal bovine serum, 100 U/ml penicillin, 100 µg/ml streptomycin and 2 mM glutamine. Up to passage 5, cells were trypsinized weekly and 800.000 cells were be seeded again in 175 cm^2 flasks. Senescence was verified by beta-Gal staining kit (LifeTechnologies; Vienna, Austria) following the manufacturer's protocol. For overexpression of genetically encoded biosensors, PAECs were infected with the BacMam 4mtD3cpv or BacMam D1ER virus (LifeTechnologies; Vienna, Austria) following the CellLight protocol. For knockdown, cells were treated with 100 nM siRNA using TransFast™ transfection reagent (Promega; Madison, WI) in serum- and antibiotic-free medium as described in the protocol. All experiments were performed 48 h after transfection or infection. siRNAs were obtained from Microsynth (Balgach, Switzerland).

2.3. mRNA Isolation and quantitative real-time polymerase chain reaction

Total RNA was isolated using the PEQLAB total RNA isolation kit (Peqlab; Erlangen, Germany) and reverse transcription was performed in a thermal cycler (Peqlab) using a cDNA synthesis kit (Applied Biosystems; Foster City, CA). mRNA levels were examined by qRT-PCR. A QuantiFast SYBR Green RT-PCR kit (Qiagen; Hilden, Germany) was used to perform real time PCR on a LightCycler 480 (Roche Diagnostics; Vienna, Austria), and data were analyzed by the REST Software (Qiagen). Relative expression of specific genes was normalized to porcine GAPDH, respectively, as a housekeeping gene. Primers for real time PCR were obtained from Invitrogen (Vienna, Austria).

2.4. Live-cell imaging experiments

Dynamic changes in $[Ca^{2+}]$mito were followed in cells expressing 4mtD3cpv. Medium was removed and cells were kept in loading buffer containing 135 mM NaCl, 5 mM KCl, 2 mM $CaCl_2$, 1 mM $MgCl_2$, 10 mM Hepes, 2.6 mM $NaHCO_3$, 440 µM KH_2PO_4, 340 µM Na_2HPO_4, 10 mM D-glucose, 0.1% vitamins, 0.2% essential amino acids, 1% penicillin/streptomycin, pH adjusted to 7.4. Single cell measurements were performed on a Zeiss AxioVert inverted microscope (Zeiss; Göttingen, Germany) equipped with a polychromator illumination system (VisiChrome, Visitron Systems; Puchheim, Germany) and a thermoelectric-cooled CCD camera (Photometrics CoolSNAP HQ, Visitron Systems; Puchheim, Germany). Infected cells were imaged with a 40 × oil-immersion objective (Zeiss). Excitation of the FRET-based genetically encoded Ca^{2+} indicator 4mtD3cpv was at 440 ± 10 nm (440AF21, Omega Optical; Brattleboro, VT), and emissions were recorded at 480 and 535 nm using emission filters (480AF30 and 535AF26, Omega Optical) mounted on a Ludl filterwheel. Devices were controlled and data were acquired by VisiView 2.0.3 (Visitron Systems) software and analyzed with GraphPad Prism version 5.00 for Windows (GraphPad Software; San Diego, CA). Results of FRET measurements are shown as (Ri – Background) + [(Ri – Background) - (R0 - Background)] (where R0 is the basal ratio) to correct for photobleaching and/or photochromism.

2.5. 3D-Colocalisation analysis

D1ER-containing adenovirus infected PAEC cells were stained for

10 min with 200 nM MitoTracker® Red CMXRos and imaged directly. High resolution images of cells were recorded by using a confocal spinning disk microscope (Axio Observer.Z1 from Zeiss, Gottingen, Germany) equipped with 100x objective lens (Plan-Fluor x100/1.45 Oil, Zeiss), a motorized filter wheel (CSUX1FW, Yokogawa Electric Corporation, Tokyo, Japan) on the emission side, AOTF-based laser merge module for laser line 405, 445, 473, 488, 561, and 561 nm (Visitron Systems) and a Nipkow-based confocal scanning unit (CSU-X1, Yokogawa Electric corporation). The D1ER and Mitotracker ® Red CMXRos were alternately excited with 488 and 561 nm laser lines, respectively, and emissions were acquired at 353 and 600 nm using a charged CCD camera (CoolSNAP-HQ, Photometrics, Tucson, AZ, USA). Z-stacks of both channels in 0.2 µm increments were recorded. The software VisiView acquisition software (Universal Imaging, Visitron Systems) was used to acquire the imaging data. Images were blind deconvoluted with NIS-elements (Nikon, Austria). The colocalization was determined on a single cell level using ImageJ and the plugin coloc2. The Pearson coefficient and the Costes tresholded Manders 1 or 2 coefficients were calculated. The MitoTracker® Red CMXRos channel was assigned to channel 1 and D1ER to channel 2.

2.6. Cell viability and apoptosis measurements

PAEC cells were seeded in 96-wells plate at a density of 5000 cells per well. Incubation with piceatannol, resveratrol, oligomycin and DMSO was started 24 h after seeding and lasted for 36 h. Cell viability was measured using CellTiter-Blue assay (Promega; Madison, WI) and apoptotic caspase activity using Caspase-Glo® 3/7 assay (Promega; Madison, WI) following the standard protocol.

2.7. Proliferation assay

For measuring the proliferation ability of cells, PAECs were seeded at a density of 5000 cells per 6-well plate well and the number of cells was counted 7 days afterwards.

2.8. NMR analysis

Metabolite levels in PAECs were determined using ^{1}H ^{1}D NMR spectroscopy. Corresponding concentrations are depicted in normalized NMR intensity units (a.u.). Probabilistic quotient normalization was performed in Matlab to correct for differences in sample metabolite dilution [20].

2.9. ROS assay

ROS production was measured using 2′,7′-dichlorodihydrofluorescein diacetate (H_2DCFDA) dye (Biotium; Hayward, CA). Cells grown until confluency in 12-well dishes were washed with warm PBS and incubated 30 min with 10 µM H_2DCFDA in PBS (37 °C). Next, the dye was aspirated, cells were washed once with cold PBS and lysed with 300 µL 3% (v/v) Triton X-100 in PBS with shaking on ice for 30 min. Then, 50 µL of cooled absolute ethanol was added to the lysate to increase the solubilization of the dye and cells were lysed for additional 15 min. Afterwards the lysates were collected and centrifuged (10 min, 13,000 rpm, 4 °C). Fluorescence was measured in duplicate in black 96-well plates at excitation and emission wavelengths of 485 and 540 nm, respectively, and normalized to protein content.

2.10. Statistics

Data shown represent the mean ± SEM. All experiments were performed using PAECs of at least three different donors. Statistical analyses were performed by using unpaired Student's *t*-test, and specific p-values are shown in the figures.

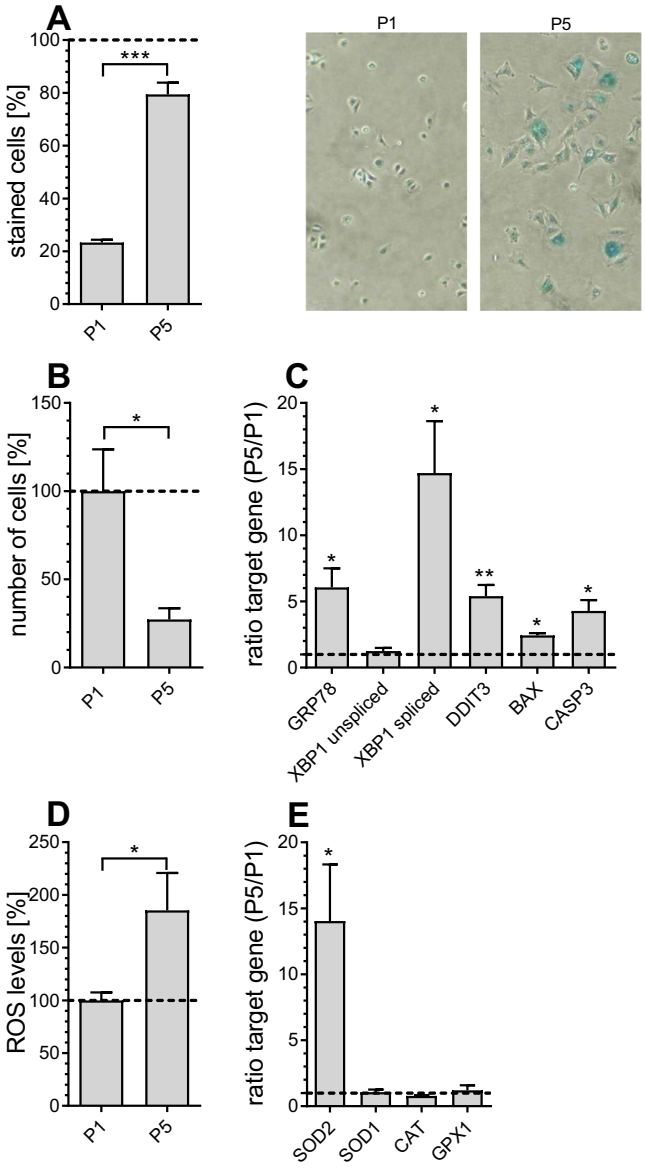

Fig. 1. Age-related markers in P1 and P5 PAECs. Percentage of β-galactosidase positively stained P1 and P5 PAECs *(left)* and representative pictures of P1 and P5 PAECs *(right)* **(A)**. Relative number of P1 and P5 PAEC 7 days after seeding, normalized to the number of P1 PAECs after 7 days **(B)**. mRNA expression ratios of GRP78, unspliced and spliced XBP1, DDIT3, BAX and CASP3 in P5 versus P1 PAECs **(C)**. Columns represent the intracellular levels of ROS production normalized to P1 PAECs **(D)**. mRNA expression ratios of SOD2, SOD1, CAT and GPX1 in P5 versus P1 PAECs **(E)**. Data are representative of ≥ 3 biological repeats ± SEM. Significant differences were assessed via unpaired *t*-test and presented as specific p-values (* = $p \leq 0.05$, ** = $p \leq 0.01$, *** = $p \leq 0.001$).

3. Results

3.1. Age-related cellular changes in an in vitro aging model

The PAEC cell *in vitro* aging model has been developed in order to mimic *in vivo* endothelial aging [19]. Senescence of PAECs was found at passage 5 and was confirmed by classical parameters including positive beta-galactosidase staining [21] (Fig. 1A), reduced proliferation rate [22] (Fig. 1B), elevated mRNA expression levels of ER stress markers [23], including glucose-regulated protein 78 (GRP78), spliced X-box binding protein 1 (XBP1), DNA damage-inducible transcript 3 protein (DDIT3), BCL2 associated X protein (BAX) and pro-apoptotic caspase 3

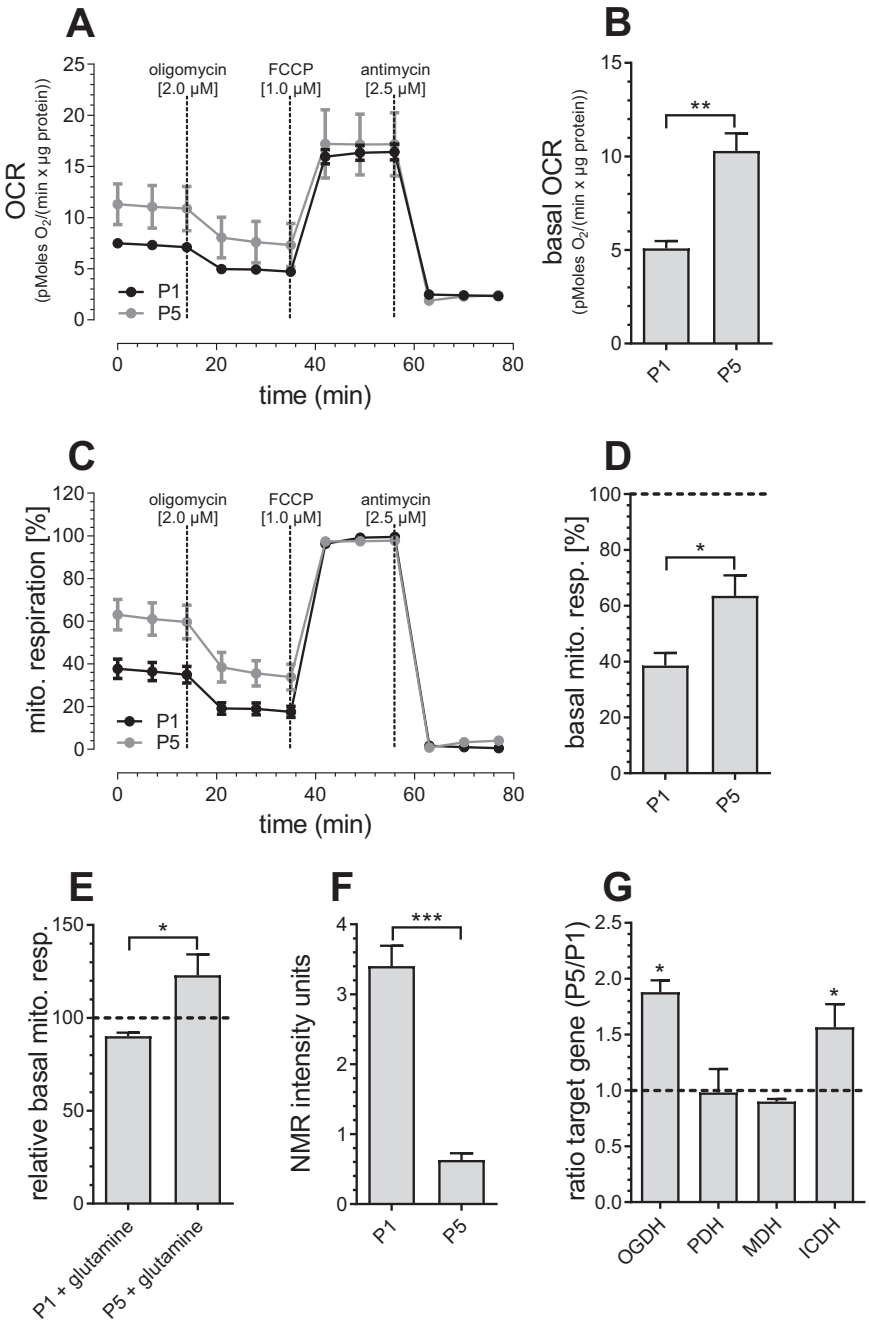

Fig. 2. Mitochondrial metabolism in P1 and P5 PAECs. Mitochondrial respiration of P1 (*black curve*) and P5 (*gray curve*) PAECs in response to oligomycin [2 µM], FCCP [1 µM] and antimycin [2.5 µM] normalized to protein content **(A)**. Bar graphs show basal mitochondrial respiration before addition of compounds **(B)**. Mitochondrial respiration of P1 *(black curve)* and P5 (*gray curve*) PAECs in response to oligomycin [2 µM], FCCP [1 µM] and antimycin [2.5 µM], normalized to maximal mitochondrial respiration **(C)**. Bar graphs show basal mitochondrial respiration presented as percentage of respective maximum mitochondrial respiration **(D)**. Basal mitochondrial respiration of P1 and P5 PAECs after 2 mM glutamine treatment, presented as percentage of basal mitochondrial respiration of respective untreated control cells **(E)**. Metabolite levels depicted as normalized NMR intensity units (a.u.) **(F)**. mRNA expression ratios of OGDH, PDH, MDH and ICDH in P5 versus P1 PAECs **(G)**. Data are representative of ≥ 3 biological repeats ± SEM. Significant differences were assessed via unpaired *t*-test and presented as specific p-values (* = $p \leq 0.05$, ** = $p \leq 0.01$, *** = $p \leq 0.001$).

(CASP3) (Fig. 1C), and increased levels of reactive oxygen species (ROS) in P5 PAECs (Fig. 1D). Consistent with high mitochondrial ROS production, mRNA expression levels of mitochondrial superoxide dismutase 2 (SOD2) were significantly increased, while there was no change in the level of cytosolic SOD (SOD1) (Fig. 1E). Notably, reports indicate that the expression or activity of ROS defense enzymes like catalase (CAT), glutathione peroxidase 1 (GPX1) and SODs is induced by ROS [24].

3.2. Enhanced mitochondrial metabolism in aged endothelial cells

Because our results are in line with the current concept pointing to the mitochondrial electron transport chain (ETC) as one of the main sources of ROS production during aging [25], we examined mitochondrial respiration changes during aging (Fig. 2A–D). The basal rate of mitochondrial respiration was found to be increased in aged endothelial cells (Figs. 2B, 2D), indicating an enhanced mitochondrial engagement to the cell's energy balance under resting conditions. Moreover, we found that basal mitochondrial respiration of senescent PAECs (P5) is significantly more dependent on glutamine than basal mitochondrial respiration of P1 PAECs (Fig. 2E). Consistent with these findings, NMR-based analysis revealed reduced glutamate levels in aged endothelial cells (Fig. 2F), possibly due to higher consumption of glutamate in the TCA cycle. This assumption was supported by increased mRNA expression levels of Ca^{2+}-dependent dehydrogenases of the TCA cycle isocitrate dehydrogenase (ICDH) and 2- oxoglutarate dehydrogenase (OGDH) in P5 PAECs, while expression of pyruvate dehydrogenase (PDH) and malate dehydrogenase (MDH) remained unchanged (Fig. 2G). These findings indicate enhanced activity of the TCA cycle, which, subsequently, fuels the ETC with electron reduction equivalents.

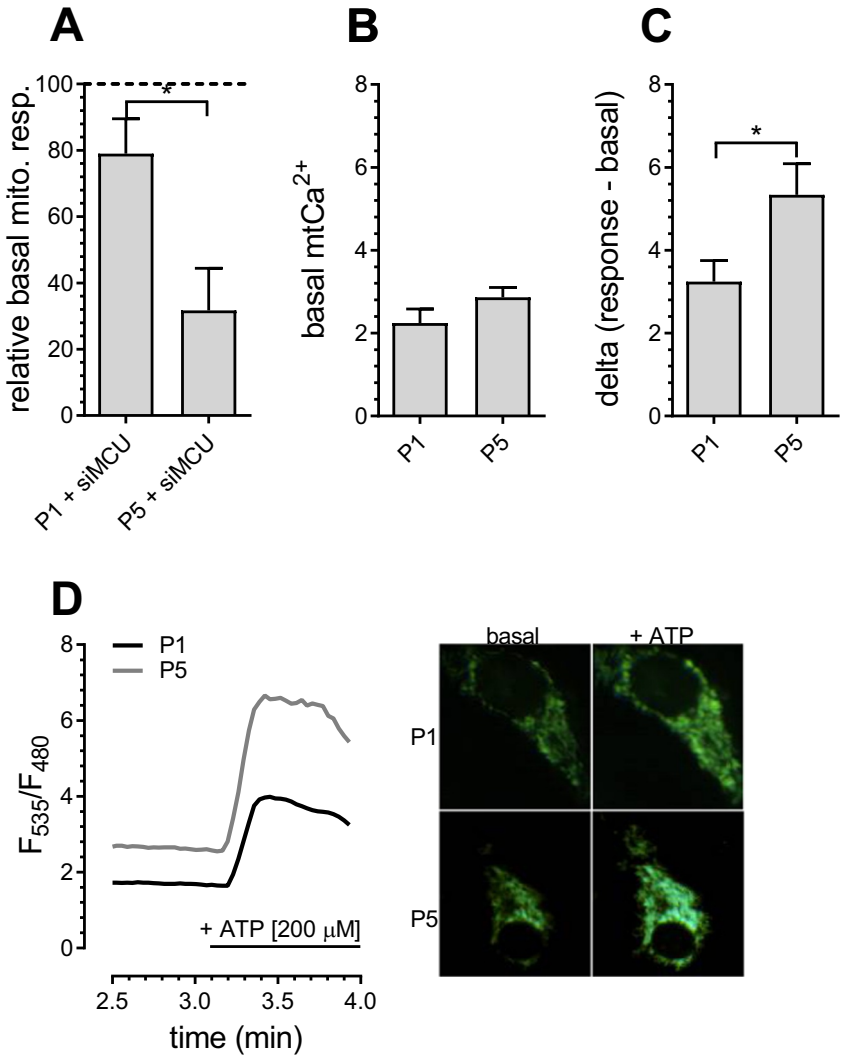

Fig. 3. Mitochondrial Ca^{2+} homeostasis in P1 and P5 PAECs. Basal mitochondrial respiration of P1 and P5 PAECs depleted of MCU (siMCU), presented as percentage of basal mitochondrial respiration of respective control cells **(A)**. Bar graphs represent basal mitochondrial Ca^{2+} levels in P1 and P5 PAECs **(B)**. Bar graphs represent mitochondrial Ca^{2+} uptake of P1 and P5 PAECs after addition of 200 µM ATP **(C)**. Representatives Ca^{2+} traces (*left*) and images (*right*) of P1 *(black curve)* and P5 *(gray curve)* PAECs expressing 4mtD3cpv **(D)**. Data (a, b, c) are representative of ≥ 3 biological repeats ± SEM. Significant differences were assessed via unpaired *t*-test and presented as specific p-values (* = $p \leq 0.05$, ** = $p \leq 0.01$, *** = $p \leq 0.001$).

3.3. Age-related changes in cellular Ca^{2+} homeostasis affect mitochondrial respiration

Since the data so far indicated an enhanced role for Ca^{2+}-dependent dehydrogenases [8], we investigated the dependency of mitochondrial respiration on mitochondrial Ca^{2+} levels and their changes during aging. Basal mitochondrial respiration of senescent P5 PAECs was significantly more affected by knockdown of the mitochondrial Ca^{2+} uniporter (MCU) than in P1 PAECs (Fig. 3A), indicating that proper mitochondrial Ca^{2+} uptake is essential for resting mitochondrial respiration in senescent endothelial cells. Notably, while resting mitochondrial Ca^{2+} was comparable in young and senescent endothelial cells (Fig. 3B), increased mitochondrial Ca^{2+} uptake was observed in P5 PAECs after IP_3-induced agonist-stimulated ER Ca^{2+} depletion (Fig. 3C, D). These data highlight an age-related increase in ER-mitochondrial Ca^{2+} transfer.

3.4. Increased ER-mitochondrial tethering as potential trigger for enhanced mitochondrial metabolism during aging

Colocalization analysis of mitochondria and ER revealed an increase in the number of contact sites between ER and mitochondria in senescent endothelial cells (Fig. 4A). Consistent with this finding, the expression of proteins associated with mitochondria-associated ER membranes (MAMs) including RAB32, AKAP1 and IP3 receptor 1 (IP3R1) were upregulated in senescent endothelial cells, while expression of the bridging proteins GRP75 and MFN2 [17] remained unchanged (Fig. 4B). The induction of enhanced mitochondrial-ER tethering by overexpression of the PKA-anchoring protein RAB32 increased mitochondrial Ca^{2+} uptake (Fig. 4C, D) and enhanced basal mitochondrial respiration (Fig. 4E) in young endothelial cells. These findings indicate that enhanced ER-mitochondrial contact is sufficient to upregulate mitochondrial Ca^{2+} transfer and mitochondrial respiration in young PAECs, mimicking conditions as in senescent PAECs.

3.5. Age-related ER stress as trigger for enhanced ER-mitochondrial linkage

Having established the co-occurrence of enhanced ER-mitochondrial Ca^{2+} transfer and enhanced mitochondrial respiration, we wondered what might be the trigger of these changes. The early phase of ER stress has already been shown previously to induce increased ER-mitochondrial coupling [26]. Since ER stress markers were found to be strongly increased in senescent PAECs (Fig. 1D), we tested whether moderate induction of ER stress induced by tunicamycin (4 h, 600 nM) mimics age-associated conditions in young endothelial cells. Moderate ER stress induced by tunicamycin increased ER-mitochondrial colocalisation (Fig. 5A), elevated the expression of MAMs-related proteins, RAB32, AKAP1 and GRP75 (Fig. 5B), and enhanced basal mitochondrial respiration (Fig. 5C). These data indicate that moderate ER stress is a potential trigger of age-related changes in this endothelial aging model.

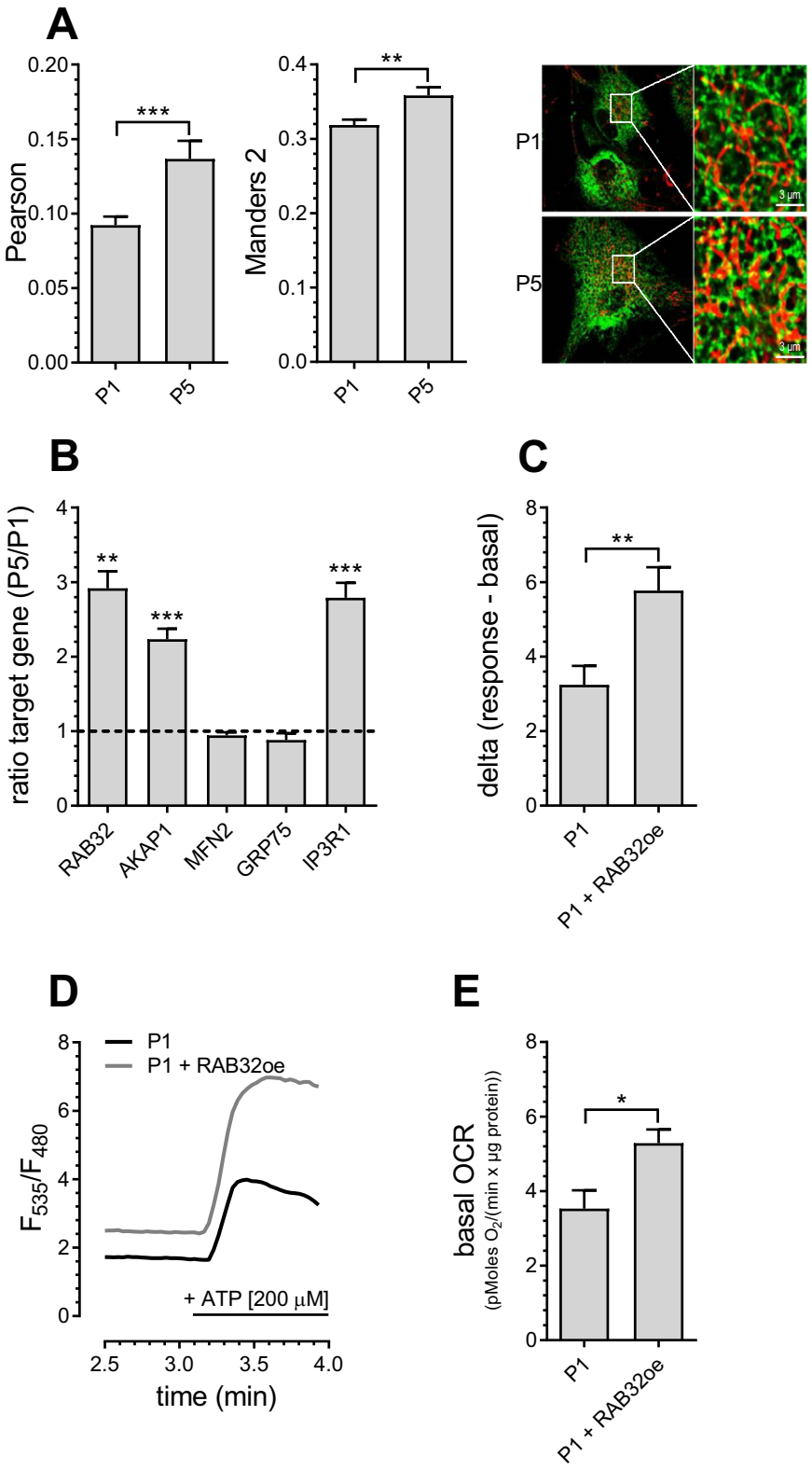

Fig. 4. Increased ER-mitochondrial contact in P5 PAECs. Co-localization of endoplasmic reticulum and mitochondria in P1 and P5 PAECs presented as Pearson *(left)* and Manders 2 *(middle)* coefficients. Representative confocal microscopy images *(right)* of P1 *(upper panel)* and P5 PAECs *(lower panel)* expressing D1ER *(green)* and stained with MitoTrackerRed® CMXRos *(red)* **(A)**. mRNA expression ratios of RAB32, AKAP1, MFN2, GRP75 and IP3R1 in P5 versus P1 PAECs **(B)**. Bar graphs represent mitochondrial Ca^{2+} uptake in P1 PAECs with and without overexpression of RAB32 after addition of 200 µM ATP **(C).** Representatives Ca^{2+} traces of P1 PAECs with *(gray curve)* or without *(black curve)* overexpression of RAB32 **(D).** Bar graphs show basal mitochondrial respiration of P1 PAECs with or without overexpression of RAB32 **(E)**. Data are representative of ≥ 3 biological repeats ± SEM. Significant differences were assessed via unpaired *t*-test and presented as specific p-values (* = $p \leq 0.05$, ** = $p \leq 0.01$, *** = $p \leq 0.001$).

3.6. Vulnerability of senescent cells to resveratrol-induced mitochondrial Ca^{2+} overload

A close proximity between ER and mitochondria was also shown to introduce an enhanced vulnerability of cancer cells to resveratrol (RSV)-induced mitochondrial Ca^{2+} overload [15]. Indeed, resveratrol, which increased mitochondrial Ca^{2+} uptake in senescent P5 PAECs significantly (Fig. 6A, B), decreased cell viability (Fig. 6C) and induced apoptotic caspase 3/7 activity (Fig. 6D) specifically in P5 PAECs, while P1 PAECs with less ER-mitochondrial contact were largely unaffected. This indicates that similar to cancer cells, the enhanced ER-mitochondrial linkage in aged PAECs renders them more susceptible to resveratrol-induced Ca^{2+}-dependent apoptosis.

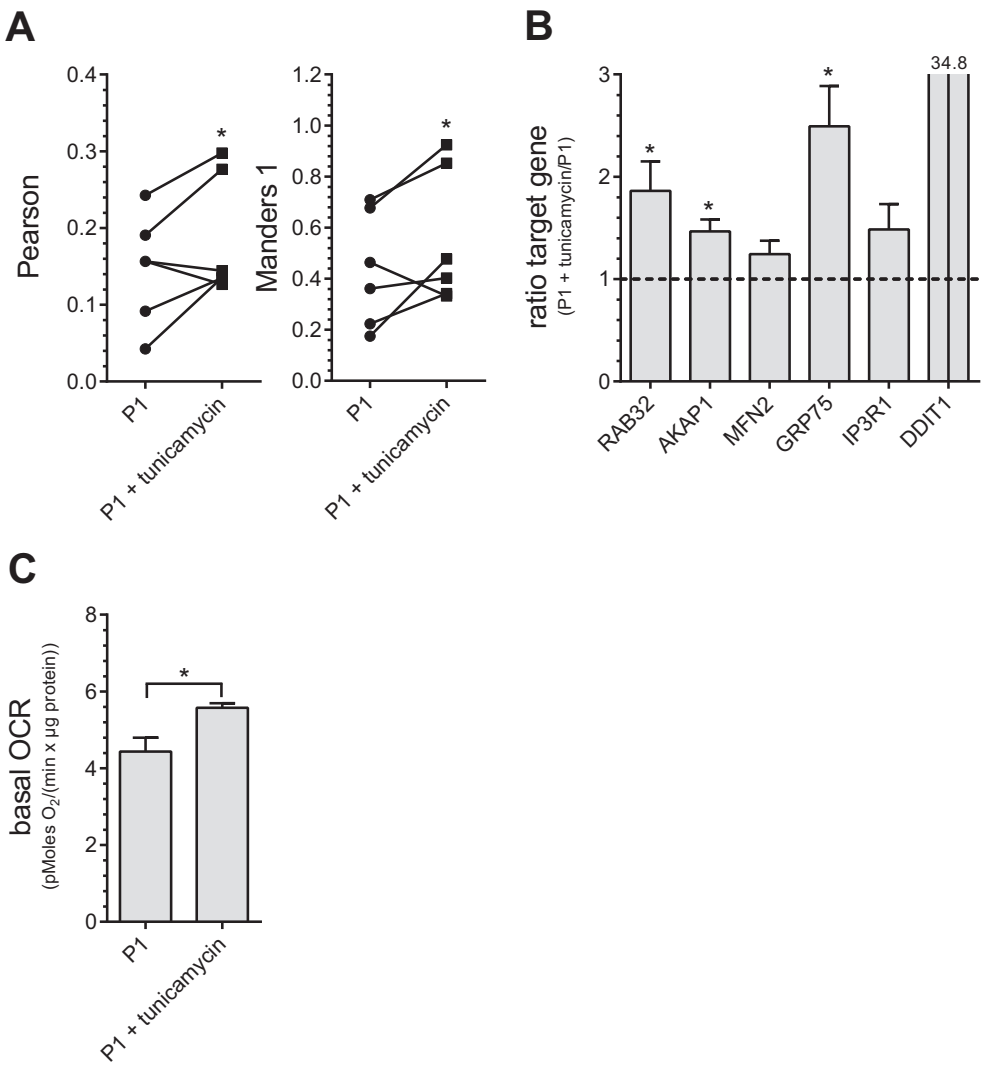

Fig. 5. Effects of ER stress on ER-mitochondrial coupling and mitochondrial metabolism. Co-localization levels of endoplasmic reticulum and mitochondria in P1 PAECs with or without treatment of tunicamycin [0.6 µM] for 4 h presented as Pearson *(left)* and Manders 1 *(right)* coefficients and analyzed via paired two sided *t*-test **(A)**. mRNA expression ratios of RAB32, AKAP1, MFN2, GRP75, IP3R1 and DDIT in P1 PAECs treated with tunicamycin versus untreated P1 PAECs **(B)**. Bar graphs represent basal mitochondrial respiration of untreated or tunicamycin-treated P1 PAECs **(C)**. All data shown are the means of ≥ 3 biological repeats ± SEM. Data are representative of ≥ 3 biological repeats ± SEM. Significant differences (b, c) were assessed via unpaired *t*-test and presented as specific p-values (* = $p \leq 0.05$, ** = $p \leq 0.01$, *** = $p \leq 0.001$).

4. Discussion

The current work supports a model in which endothelial cell aging is accompanied by ER stress-enhanced ER-mitochondrial tethering and consequently an increase in inter-organellar Ca^{2+} transfer and activity of mitochondrial respiration. Senescence of this *in vitro* aging model was approved by classical aging markers including positive beta-galactosidase staining and reduced proliferation rate amongst others. Nevertheless, additional differentiation processes that occur in primary cells after several passages in culture and have been described for vascular smooth muscle cells can't be excluded [27].

Our results concerning increased mitochondrial activity and enhanced ER-mitochondrial Ca^{2+} flux during cellular aging are consistent with former *in vitro* aging studies, including an aging model based on rat hippocampal neurons [28]. A biphasic mitochondrial aging process has been reported for animals including mice, monkeys and drosophila. In the biphasic model, increased mitochondrial activity during middle age is followed by a decline in mitochondrial activity, potentially caused by detrimental ROS production during middle age combined with a loss of ROS defense mechanisms as aging progresses [2]. We speculate that *in vitro,* a homogeneously aged cell population occurs, while the aging state of individual cells in living animals might be more diverse. These differences might explain the nearly sudden growth arrest in *in vitro* aging models as opposed to the slow decrease in physiological functions in animals. Notably, we found strongly increased SOD2 levels, reflecting proper ROS defense, in the senescent PAECs although these cells were close to growth arrest. This might be due to artificial selection caused by cell passage. In the case of a cell with strongly increased ROS production without proper defense, it is likely to lose its adherence and therefore be eliminated during passage. This selection coupled with growth arrest at old age lead us to speculate that cellular aging model used in this study does not reflect the stage of old-age but more likely represent mechanisms occurring during middle age.

A previous study associated low levels of ER stress with ER-mitochondrial colocalization [26], implying that increased ER-mitochondrial coupling may be a cellular protection mechanism against ER stress. Since ER stress markers were strongly elevated in senescent PAECs, it seemed reasonable to test whether this was in fact driving the observed increased ER-mitochondrial communication in the senescent PAECs. In support of this notion, tunicamycin-induced moderate ER stress induced mitochondria-ER colocalization in young PAECs. However, the underlying molecular mechanism of this relationship is still elusive. One possible explanation might be that Ca^{2+} hotspots on the surface of the ER caused by ER-stress induced Ca^{2+} leak results in localized conformational changes and functional activation of the proteins involved in ER-mitochondrial tethering. Furthermore, ER-stress induced activation of various transcription factors such as NFEL2L or HIF1alpha are possible. These molecular mechanisms have to be further elaborated in order to clarify the reason for increased ER-mitochondrial crosstalk during aging.

The ER has been found to lack efficiency during age, resulting in ER dysfunction and impaired protein synthesis [29]. Increased ER-

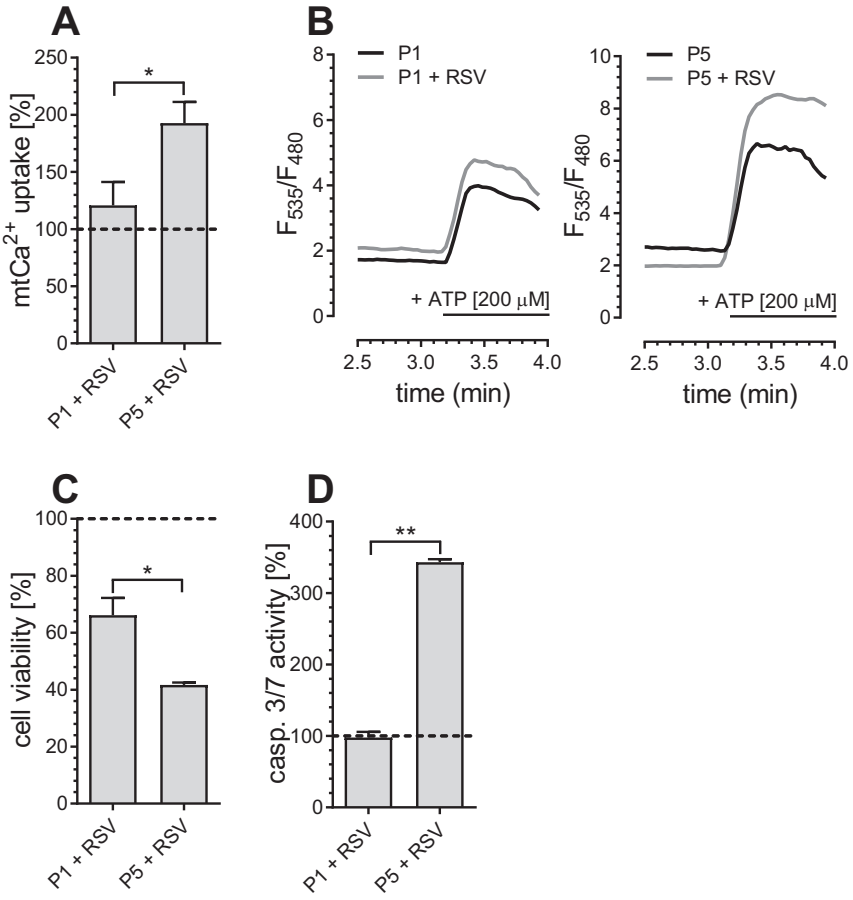

Fig. 6. Resveratrol sensitizes aged PAECs to mitochondrial Ca^{2+} overload-induced apoptosis. Bar graphs represent mitochondrial Ca^{2+} uptake after addition of 200 μM ATP in P1 and P5 PAECs treated with resveratrol (RSV) [100 μM], normalized to mitochondrial Ca^{2+} uptake of untreated control cells **(A)**. Representatives Ca^{2+} traces of P1 and P5 PAECs treated *(gray curves)* or not treated *(black curves)* with 100 μM resveratrol (RSV) **(B)**. Cell viability of P1 and P5 PAECs after 36 h of incubation with resveratrol (RSV) [100 μM], calculated as percentage of viable cells in comparison to corresponding untreated control cells **(C)**. Caspase 3/7 activity of P1 and P5 PAECs, normalized to corresponding untreated control cells and presented as percentage **(D)**. Data shown (a, c, d) are the means of ≥ 3 biological repeats ± SEM. Data are representative of ≥ 3 biological repeats ± SEM. Significant differences were assessed via unpaired *t*-test and presented as specific p-values (* = $p \leq 0.05$, ** = $p \leq 0.01$, *** = $p \leq 0.001$).

mitochondrial linkage and Ca^{2+} crosstalk during aging might help to boost mitochondrial ATP production, which in turn might help to temporarily prolong ER function as cells age. Nevertheless, ROS will be produced as side-products. Consequently, enhanced mitochondrial metabolism to boost ER ATP levels might be fruitful for the cell only as long as a certain ROS level is not exceeded and ROS defense mechanisms are still intact, but could lead aging cells eventually into detrimental ROS production and damage.

Our data show that senescent cells with enhanced ER-mitochondrial linkage are more susceptible to resveratrol-induced mitochondrial Ca^{2+} overload and cell death, which is consistent with the mechanism proposed for cancer cells [15].

A potential life-prolonging effect of resveratrol has been investigated since the beginning of the 1990s. At this time, the research on resveratrol was largely boosted by the so-called “French paradox”, describing the low incidence of coronary heart diseases in French people despite their high intake of saturated fatty acids. resveratrol-rich red wine was proposed to protect French people by inducing anti-oxidant effects, which is still under debate since conclusive studies are missing [2]. Notably, resveratrol treatment was reported to significantly diminish the senescence-associated secretory phenotype (SASP) in senescent human fibroblasts [30]. Reduction of the SASP phenotype was also associated with the senolytic function of the polyphenol quercetin, one of the first senolytic drugs identified and recently also proven to enhance health- and lifespan in old mice in combination with dasatinib [31]. Targeting senescence-associated mitochondrial dysfunction has been suggested as possible mechanisms of senolytic drugs [32]. Consistent with this assumption, we propose that increased risk for mitochondrial Ca^{2+} overload due to enhanced ER-mitochondrial tethering, might be an Achilles' heel of an senescent cell and might offer the possibility to develop Ca^{2+} overload-selective senolytic drugs, which cause a clearance of certain aged cells and thereby reduce the systemic pathogenic effects of senescent cells [33].

A detailed knowledge of the changes and regulatory mechanisms of mitochondrial Ca^{2+} uptake during senescence seem to be essential for better understanding of the cellular aging process and aging-related diseases. Since cardiovascular diseases are the main cause of death, an in-depth understanding of the endothelial aging process is of major importance. Using a porcine aortic endothelial cell model, this study contributed to a greater understanding of endothelial aging by revealing changes in ER-mitochondrial crosstalk that may act as a trigger for altered function of both organelles with significant consequences for cell survival during aging.

Acknowledgements

We greatly thank Ms. Nathalie Carpentier and Ms. Emilie Royere for their excellent technical support. Moreover, we thank Dr. Jesse Hay, University of Montana, for proofreading our manuscript. This work was funded by the Austrian Science Funds (FWF, DKplus W 1226-B18 and J4205-B27). C.T.M. and C.K. were doctoral fellows within the doctoral programme Metabolic and Cardiovascular Disease (FWF, DKplus W 1226-B18) and C.T.M. is currently funded by an Erwin Schroedinger Abroad Fellowship (J4205-B27).

References

[1] C. Lopez-Otin, M.A. Blasco, L. Partridge, M. Serrano, G. Kroemer, The hallmarks of aging, Cell 153 (6) (2013) 1194–1217, https://doi.org/10.1016/j.cell.2013.05.039.
[2] C.T. Madreiter-Sokolowski, A.A. Sokolowski, M. Waldeck-Weiermair, R. Malli, W.F. Graier, Targeting mitochondria to counteract age-related cellular dysfunction, Genes 9 (3) (2018), https://doi.org/10.3390/genes9030165.
[3] D.J. Baker, S. Peleg, Biphasic modeling of mitochondrial metabolism dysregulation during aging, Trends Biochem. Sci. 42 (9) (2017) 702–711, https://doi.org/10.

1016/j.tibs.2017.06.005.
[4] T.D. Pugh, M.W. Conklin, T.D. Evans, M.A. Polewski, H.J. Barbian, R. Pass, B.D. Anderson, R.J. Colman, K.W. Eliceiri, P.J. Keely, R. Weindruch, T.M. Beasley, R.M. Anderson, A shift in energy metabolism anticipates the onset of sarcopenia in rhesus monkeys, Aging Cell 12 (4) (2013) 672–681, https://doi.org/10.1111/acel.12091.
[5] D.V. Ziegler, C.D. Wiley, M.C. Velarde, Mitochondrial effectors of cellular senescence: beyond the free radical theory of aging, Aging Cell 14 (1) (2015) 1–7, https://doi.org/10.1111/acel.12287.
[6] M.D. Bruss, C.F. Khambatta, M.A. Ruby, I. Aggarwal, M.K. Hellerstein, Calorie restriction increases fatty acid synthesis and whole body fat oxidation rates, Am. J. Physiol. Endocrinol. Metab. 298 (1) (2010) E108–E116, https://doi.org/10.1152/ajpendo.00524.2009.
[7] C. Correia-Melo, F.D. Marques, R. Anderson, G. Hewitt, R. Hewitt, J. Cole, B.M. Carroll, S. Miwa, J. Birch, A. Merz, M.D. Rushton, M. Charles, D. Jurk, S.W. Tait, R. Czapiewski, L. Greaves, G. Nelson, Y.M. Bohlooly, S. Rodriguez-Cuenca, A. Vidal-Puig, D. Mann, G. Saretzki, G. Quarato, D.R. Green, P.D. Adams, T. von Zglinicki, V.I. Korolchuk, J.F. Passos, Mitochondria are required for pro-ageing features of the senescent phenotype, EMBO J. 35 (7) (2016) 724–742, https://doi.org/10.15252/embj.201592862.
[8] R.M. Denton, P.J. Randle, B.J. Bridges, R.H. Cooper, A.L. Kerbey, H.T. Pask, D.L. Severson, D. Stansbie, S. Whitehouse, Regulation of mammalian pyruvate dehydrogenase, Mol. Cell. Biochem. 9 (1) (1975) 27–53.
[9] C.T. Madreiter-Sokolowski, A.A. Sokolowski, W.F. Graier, Dosis Facit Sanitatem-concentration-dependent effects of resveratrol on mitochondria, Nutrients 9 (10) (2017), https://doi.org/10.3390/nu9101117.
[10] M. McKenzie, S.C. Lim, M.R. Duchen, Simultaneous measurement of mitochondrial calcium and mitochondrial membrane potential in live cells by fluorescent microscopy, J. Vis. Exp. (119) (2017), https://doi.org/10.3791/55166.
[11] C.T. Madreiter-Sokolowski, C. Klec, W. Parichatikanond, S. Stryeck, B. Gottschalk, S. Pulido, R. Rost, E. Eroglu, N.A. Hofmann, A.I. Bondarenko, T. Madl, M. Waldeck-Weiermair, R. Malli, W.F. Graier, PRMT1-mediated methylation of MICU1 determines the UCP2/3 dependency of mitochondrial Ca^{2+} uptake in immortalized cells, Nat. Commun. 7 (2016) 12897, https://doi.org/10.1038/ncomms12897.
[12] S. Naghdi, M. Waldeck-Weiermair, I. Fertschai, M. Poteser, W.F. Graier, R. Malli, Mitochondrial Ca^{2+} uptake and not mitochondrial motility is required for STIM1-Orai1-dependent store-operated Ca^{2+} entry, J. Cell Sci. 123 (Pt 15) (2010) 2553–2564, https://doi.org/10.1242/jcs.070151.
[13] M. Waldeck-Weiermair, M.R. Alam, M.J. Khan, A.T. Deak, N. Vishnu, F. Karsten, H. Imamura, W.F. Graier, R. Malli, Spatiotemporal correlations between cytosolic and mitochondrial Ca^{2+} signals using a novel red-shifted mitochondrial targeted cameleon, PLoS One 7 (9) (2012) e45917, https://doi.org/10.1371/journal.pone.0045917.
[14] A. Raturi, T. Simmen, Where the endoplasmic reticulum and the mitochondrion tie the knot: the mitochondria-associated membrane (MAM), Biochim. Biophys. Acta 1833 (1) (2013) 213–224, https://doi.org/10.1016/j.bbamcr.2012.04.013.
[15] C.T. Madreiter-Sokolowski, B. Gottschalk, W. Parichatikanond, E. Eroglu, C. Klec, M. Waldeck-Weiermair, R. Malli, W.F. Graier, Resveratrol specifically kills cancer cells by a devastating increase in the Ca^{2+} coupling between the greatly tethered endoplasmic reticulum and mitochondria, Cell Physiol. Biochem. 39 (4) (2016) 1404–1420, https://doi.org/10.1159/000447844.
[16] K. Samanta, S. Douglas, A.B. Parekh, Mitochondrial calcium uniporter MCU supports cytoplasmic Ca2+ oscillations, store-operated Ca^{2+} entry and Ca^{2+}-dependent gene expression in response to receptor stimulation, PLoS One 9 (7) (2014) e101188, https://doi.org/10.1371/journal.pone.0101188.
[17] M. Bui, S.Y. Gilady, R.E. Fitzsimmons, M.D. Benson, E.M. Lynes, K. Gesson, N.M. Alto, S. Strack, J.D. Scott, T. Simmen, Rab32 modulates apoptosis onset and mitochondria-associated membrane (MAM) properties, J. Biol. Chem. 285 (41) (2010) 31590–31602, https://doi.org/10.1074/jbc.M110.101584.
[18] C. Fernandez-Sanz, M. Ruiz-Meana, E. Miro-Casas, E. Nunez, J. Castellano, M. Loureiro, I. Barba, M. Poncelas, A. Rodriguez-Sinovas, J. Vazquez, D. Garcia-Dorado, Defective sarcoplasmic reticulum-mitochondria calcium exchange in aged mouse myocardium, Cell Death Dis. 5 (2014) e1573, https://doi.org/10.1038/cddis.2014.526.
[19] E. Perrier, M.P. Fournet-Bourguignon, E. Royere, S. Molez, H. Reure, L. Lesage, W. Gosgnach, Y. Frapart, J.L. Boucher, N. Villeneuve, J.P. Vilaine, Effect of uncoupling endothelial nitric oxide synthase on calcium homeostasis in aged porcine endothelial cells, Cardiovasc. Res. 82 (1) (2009) 133–142, https://doi.org/10.1093/cvr/cvp034.
[20] F. Dieterle, A. Ross, G. Schlotterbeck, H. Senn, Probabilistic quotient normalization as robust method to account for dilution of complex biological mixtures. Application in 1H NMR metabonomics, Anal. Chem. 78 (13) (2006) 4281–4290, https://doi.org/10.1021/ac051632c.
[21] Y.Q. Geng, J.T. Guan, X.H. Xu, Y.C. Fu, Senescence-associated beta-galactosidase activity expression in aging hippocampal neurons, Biochem. Biophys. Res. Commun. 396 (4) (2010) 866–869, https://doi.org/10.1016/j.bbrc.2010.05.011.
[22] Y. Zu, L. Liu, M.Y. Lee, C. Xu, Y. Liang, R.Y. Man, P.M. Vanhoutte, Y. Wang, SIRT1 promotes proliferation and prevents senescence through targeting LKB1 in primary porcine aortic endothelial cells, Circ. Res. 106 (8) (2010) 1384–1393, https://doi.org/10.1161/CIRCRESAHA.109.215483.
[23] M.K. Brown, N. Naidoo, The endoplasmic reticulum stress response in aging and age-related diseases, Front. Physiol. 3 (2012) 263, https://doi.org/10.3389/fphys.2012.00263.
[24] L. Miao, D.K. St Clair, Regulation of superoxide dismutase genes: implications in disease, Free Radic. Biol. Med. 47 (4) (2009) 344–356, https://doi.org/10.1016/j.freeradbiomed.2009.05.018.
[25] M.P. Murphy, How mitochondria produce reactive oxygen species, Biochem J. 417 (1) (2009) 1–13, https://doi.org/10.1042/BJ20081386.
[26] R. Bravo, J.M. Vicencio, V. Parra, R. Troncoso, J.P. Munoz, M. Bui, C. Quiroga, A.E. Rodriguez, H.E. Verdejo, J. Ferreira, M. Iglewski, M. Chiong, T. Simmen, A. Zorzano, J.A. Hill, B.A. Rothermel, G. Szabadkai, S. Lavandero, Increased ER-mitochondrial coupling promotes mitochondrial respiration and bioenergetics during early phases of ER stress, J. Cell Sci. 124 (Pt 13) (2011) 2143–2152, https://doi.org/10.1242/jcs.080762.
[27] E. Munoz, M. Hernandez-Morales, D. Sobradillo, A. Rocher, L. Nunez, C. Villalobos, Intracellular Ca(2+) remodeling during the phenotypic journey of human coronary smooth muscle cells, Cell Calcium 54 (5) (2013) 375–385, https://doi.org/10.1016/j.ceca.2013.08.006.
[28] M. Calvo-Rodriguez, M. Garcia-Durillo, C. Villalobos, L. Nunez, In vitro aging promotes endoplasmic reticulum (ER)-mitochondria Ca^{2+} cross talk and loss of store-operated Ca^{2+} entry (SOCE) in rat hippocampal neurons, Biochim. Biophys. Acta 1863 (11) (2016) 2637–2649, https://doi.org/10.1016/j.bbamcr.2016.08.001.
[29] G. Martinez, C. Duran-Aniotz, F. Cabral-Miranda, J.P. Vivar, C. Hetz, Endoplasmic reticulum proteostasis impairment in aging, Aging Cell 16 (4) (2017) 615–623, https://doi.org/10.1111/acel.12599.
[30] V. Pitozzi, A. Mocali, A. Laurenzana, E. Giannoni, I. Cifola, C. Battaglia, P. Chiarugi, P. Dolara, L. Giovannelli, Chronic resveratrol treatment ameliorates cell adhesion and mitigates the inflammatory phenotype in senescent human fibroblasts, J. Gerontol. A Biol. Sci. Med. Sci. 68 (4) (2013) 371–381, https://doi.org/10.1093/gerona/gls183.
[31] M. Xu, T. Pirtskhalava, J.N. Farr, B.M. Weigand, A.K. Palmer, M.M. Weivoda, C.L. Inman, M.B. Ogrodnik, C.M. Hachfeld, D.G. Fraser, J.L. Onken, K.O. Johnson, G.C. Verzosa, L.G.P. Langhi, M. Weigl, N. Giorgadze, N.K. LeBrasseur, J.D. Miller, D. Jurk, R.J. Singh, D.B. Allison, K. Ejima, G.B. Hubbard, Y. Ikeno, H. Cubro, V.D. Garovic, X. Hou, S.J. Weroha, P.D. Robbins, L.J. Niedernhofer, S. Khosla, T. Tchkonia, J.L. Kirkland, Senolytics improve physical function and increase lifespan in old age, Nat. Med. 24 (8) (2018) 1246–1256, https://doi.org/10.1038/s41591-018-0092-9.
[32] J.L. Kirkland, T. Tchkonia, Cellular senescence: a translational perspective, EBioMedicine 21 (2017) 21–28, https://doi.org/10.1016/j.ebiom.2017.04.013.
[33] J.L. Kirkland, T. Tchkonia, Y. Zhu, L.J. Niedernhofer, P.D. Robbins, The clinical potential of senolytic drugs, J. Am. Geriatr. Soc. (2017), https://doi.org/10.1111/jgs.14969.